Precision Measurement and Mapping of Die-Attach Thermal Resistance

Katsuo Kurabayashi and Kenneth E. Goodson

***Abstract*—The thermal resistance of the attachment between a die and its carrier contributes strongly to the total temperature rise in an electronic system. The die attach resistance often differs substantially from the value predicted using the bulk thermal conductivity of the attachment material because of partial voiding and delamination. These defects can be introduced during the attachment process or during subsequent exposure to humidity or temperature fluctuations. This manuscript develops a technique for precisely measuring the spatially-averaged die-attach thermal resistance and for mapping spatial variations of the resistance in the plane of the die. The spatially-averaged resistance measurements use transient electrical heating and thermometry at frequencies up to 1 kHz to achieve a value of the uncertainty near 10^{-6} m^2K/W, which is a substantial improvement over existing steady-state methods. Spatial variations are captured using scanning laser-reflectance thermometry and a deconvolution method detailed here. The data in this manuscript show the impact of the adhesive material, the adhesive thickness, and the attachment pressure on the thermal resistance, as well as the spatial variation of the resistance resulting from incomplete contact.**

***Index Terms*— Die attachment, die-attach adhesives, electrical resistance thermometry, packaging design, photothermal reflectance thermometry, thermal resistance.**

I. Introduction

THERMAL conduction in an electronic system is strongly impeded by the thermal resistance at the die-carrier attachment. This resistance causes a large temperature rise in transistors and interconnects and leads to a shorter chip lifetime [1]. The growing dimensions of chips used in electronic systems are increasing the problems of voiding and partial delamination in the attachment [2]. These defects augment the die-attach thermal resistance and make the packaging less reliable. The die-attach thermal resistance depends strongly on the materials used for adhesion and the temperature history experienced by the electronic assembly, as well as the manner in which adhesive is applied. Bulk data for the thermal properties of adhesive materials are usually not appropriate for predicting the die-attach thermal resistance because they do not account for voiding, partial delamination, and stoichiometric changes that occur during the processing and lifetime of an attachment. For polymer attachments that are filled with metal particles, such as silver-filled epoxy, the bulk thermal conductivity data do not account for the change in volume fraction that can occur during the attachment process. For these reasons, precise measurements of the die-attach thermal resistance are needed to support accurate thermal simulations of electronic packages.

There have been several important studies on thermal conduction through die-carrier interfaces. Pfannschmidt [3] studied the thermal resistance in die attachments of varying quality using diode thermometers and steady-state heating. The thermal resistance data were interpreted with the help of scanning acoustic microscopy (SAM), which imaged local voids and regions of incomplete contact in the plane of the die. The data were particularly sensitive to defects directly between the diode temperature sensors. Beyfuss *et al*. [4] used photothermal microscopy to observe variations in the local thermal resistance for a silicon chip, which was partially bonded on a sapphire substrate such that an air gap remained over a fraction of the interface area. The air-gap thickness was altered using a piezoelectric actuator and measured using laser interferometry. Beyfuss *et al*. [4] measured the phase shift of the photothermal data for the silicon die temperature as a function of the air gap thickness, which allowed the thermal resistance resulting from the gap thickness to be qualitatively determined. Both of these studies provided qualitative information about the impact of delamination on the thermal resistance. However, there remains a need for a technique that precisely measures both the spatially-averaged thermal resistance and its variations within the plane of the die. Such a technique is needed to assess the quality of new attachment materials and procedures and would yield data that could be directly imported into finite-element simulations of packages.

The present work develops an experimental technique that meets these demands. The measurement approach uses:

1) frequency-domain electrical heating/thermometry;
2) scanning photothermal imaging.

The technique 1) is used to extract the spatially-averaged die-attach thermal resistance from the temperature-rise response at the die surface during transient heating. The technique 2) yields photothermal images showing variations in the temperature-rise magnitude due to spatial variations in the die attach thermal resistance. In contrast to previous photothermal studies, the present work uses the data for the spatially-averaged die-attach thermal resistance to extract quantitative values of thermal resistance variation from the images. Data are reported for a variety of dielectric attachments and are compared with x-ray images, which provide information about the mechanical quality of the attachment.

Manuscript received August 1, 1998. This work was supported by the Semiconductor Research Corporation under Contract 98-PJ-357 and 98-SJ-461, Office of Naval Research Young Investigator Award, and the National Science Foundation CAREER Award. This paper was recommended for publication by Associate Editor M. Tirumala upon evaluation of the reviewers' comments.

The authors are with Stanford University, Stanford, CA 94305 USA.

Publisher Item Identifier S 1070-9886(98)07999-2.

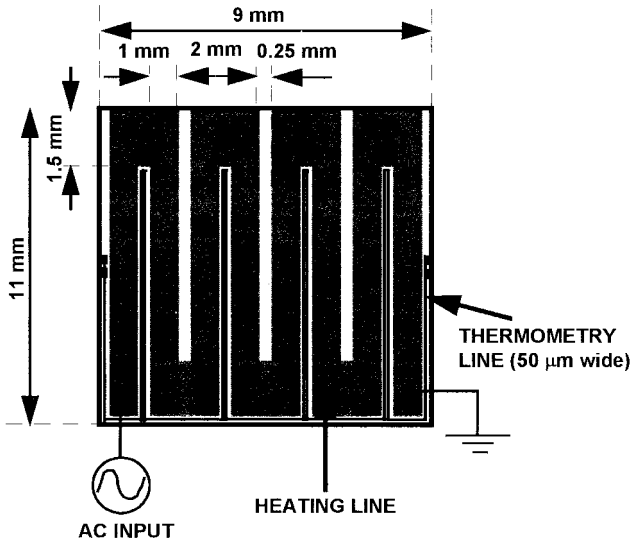

Fig. 1. Thermometry structure patterned on the silicon die. The four-point-contact technique is used for measuring the electrical resistance change of the thermometry line with temperature.

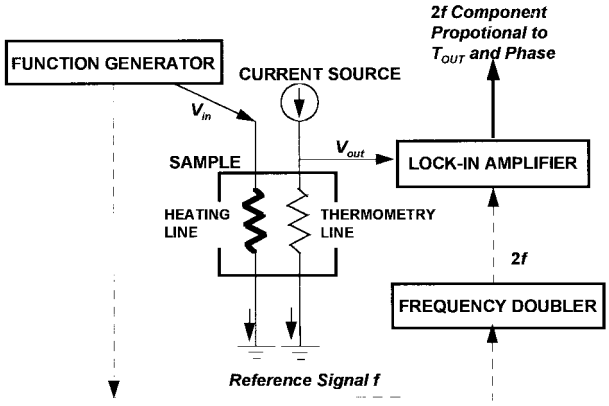

Fig. 2. Experimental setup for the spatially-averaged die-attach thermal resistance measurement using the die in Fig. 1.

II. Measurement of the Spatially-Averaged Die-Attach Thermal Resistance

This measurement uses periodic electrical heating and thermometry in metal lines on the die surface at frequencies between 10 and 1000 Hz to measure thermal resistance at the interfaces of the silicon die and the carrier. A layer of silicon dioxide is thermally grown on the silicon die, and gold bridges are patterned onto the oxide layer using photolithography, yielding the structures shown in Fig. 1. A large periodic current sustained in the wide bridge heats the die surface and the narrow bridge, which carries a low current and induces negligible Joule heating, is used for simultaneous electrical-resistance thermometry. The die is attached to an aluminum-oxide carrier using one of several different adhesives and attachment pressures, which are discussed in greater detail in this section. Fig. 2 shows the configuration of the apparatus used for this measurement. The periodic current I at frequency f in the heating line yields transient heating at the frequency $2f$, which is well approximated by $P = I^2 R_0$. The electrical resistance R_0 is the time-averaged value for the heating line, which is very nearly equal to its electrical resistance at the time-averaged temperature during the measurement. The electrical resistance of the narrow bridge fluctuates in response to the heating and is measured using the lock-in amplifier and a steady-state bias current of 1 mA, which yields a current density of 8×10^7 A m^{-2}. The lock-in amplifier provides the amplitude and phase of the temperature fluctuations, which are used together with the analysis provided later in this section to extract the spatially-averaged die-carrier thermal resistance.

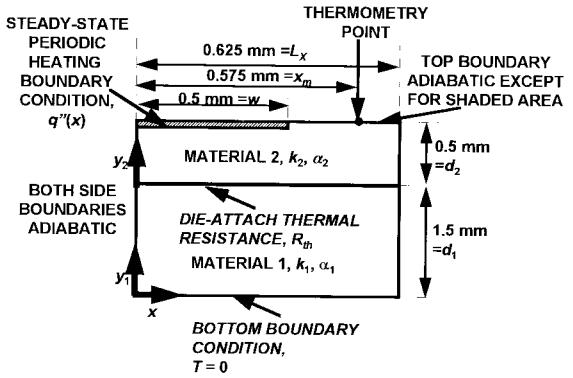

Fig. 3. Geometry and boundary condition used for the thermal modeling. The materials 1 and 2 are the Al_2O_3 carrier and the silicon die, respectively. The calculation used $k_1 = 20$ W/mK; $k_2 = 100$ W/mK; $1 = 5 \times 10^{-6}$ m^2/s; and $2 = 5 \times 10^{-5}$ m^2/s.

The primary benefit of using a transient approach results from the fact that the volume of interrogated material can be confined to the die and a portion of the carrier, such that the boundary conditions for the carrier exert negligible influence. These boundary conditions, which are difficult to predict and reproduce, strongly influence the temperature rises measured in a steady-state experiment. Although steady-state measurements can compensate for this difficulty through the use of a second thermometer in the carrier, the unknown boundary conditions continue to influence both thermometry signals and the measurement uncertainty. The maximum extent of heat penetration for the present study occurs at 10 Hz, for which the Fourier number defined using the silicon die thickness and the heating period is much larger than unity. However, the penetration depth in the carrier for 10 Hz is about 0.7 mm, which is less than the half of the total carrier thickness. This means that the boundary condition at the bottom surface of the carrier does not influence the temperature amplitude and phase data at the top surface of the die. When the heating frequency is near 200 Hz, the penetration depth in the silicon is comparable with the silicon die thickness of 500 μm.

Fig. 3 shows the geometry and the boundary conditions used for simulating thermal conduction in the sample structure. The sides of the simulation domain are modeled as adiabatic to describe the spatial periodicity of the heating. Although the heating is volumetric within the metal, it is well approximated as a heat flux boundary condition at the top surface of the silicon die when:

1) the heat capacity of metal is negligible compared to that of the heated domain within the die and carrier;

2) lateral spreading of heat in the oxide layer between the line and the die is negligible;
3) lateral spreading of heat in the metal is negligible.

Condition 1) is satisfied at even the highest frequencies used in the present work, since the volume heated in the silicon is much larger than the volume of the metal. Condition 2) is satisfied because the ratio of the width of the heating bridge is larger than the thickness of the silicon dioxide by more than three orders of magnitude. Condition 3) is satisfied because the lateral thermal healing length in the metal, which describes the length over which lateral conduction spreads the generated heat, is approximately two orders of magnitude smaller than the total width of the metal bridge.

Heat transfer from the top surface of the die to the ambient air is neglected. This is justified by the large value of the die-to-carrier thermal conductance compared to the die-to-ambient thermal conductance accounting for natural convection and radiation. By considering the maximum extent of heat penetration and assuming one-dimensional heat conduction in the carrier, a lower bound for the die-to-carrier conductance is estimated to be $G \sim A_d/(L_{\text{carrier}}/k_{\text{carrier}} + R^u_{\text{th}}) = 1.1 \times 10^{-1}$ W K^{-1}, where $A_d = 10^{-4}$ m^2 is the total die surface area, $k_{\text{carrier}} = 20$ W K^{-1} m^{-1} is the thermal conductivity of the carrier material, $L_{\text{carrier}} = 0.7$ mm is the maximum heat penetration depth in the carrier at 10 Hz, $R^u_{\text{th}} = 9 \times 10^{-4}$ m^2 K W^{-1} is the upper bound for the die-attach thermal resistance measured in this study. The thermal conductance contributed by the air convection at the top surface of the die is estimated based on a numerical study of natural convection above a uniformly heated horizontal plate [5]. Using room-temperature properties and the die geometries yields the Rayleigh number, $\text{Ra}_L = g\beta(T_m - T_0)L^{*3}/\nu_a\alpha_a = 85$, where g is the acceleration due to gravity, $T_m = 363$ K is the largest temperature at the top surface of the die during the measurement, $T_0 = 293$ K is room temperature, and $\beta \sim 2/(T_0 + T_m)$ is the approximate thermal expansion coefficient of the air, L^* is the characteristic lateral length of the die, which is given by $L^* = A_d/P$, where P is the perimeter of the total die surface area, ν_a is the kinematic viscosity of the air, and α_a is the thermal diffusivity of the air. The average Nusselt number, $\overline{\text{Nu}}$, is approximately 2 for $\text{Ra}_{L.} = 85$ [5], which yields a conductance due to natural convection $G = \overline{\text{Nu}}k_aA_d/L^* = 2.1 \times 10^{-3}$ W K^{-1}, where k_a is the thermal conductivity of the air at room temperature. The thermal conductance due to radiation is on the order of $G = 4\varepsilon\sigma T_H^3 A$, where ε is the emissivity, σ is the Stefan–Boltzmann constant, and A is the area of the emitting surface. Using $\varepsilon = 1$ for an upper bound and $A = A_d$ yields $G = 2.7 \times 10^{-4}$ W K^{-1} at room temperature. The conductances from the top surface of the die due to natural convection and radiation are both much smaller than that for conduction into the carrier.

The dimensions, $2L_x = 1.25$ mm and $2w = 1$ mm, are respectively the center-to-center distance between the adjacent heating stripes and the heating-line width. The governing heat conduction equations are

$$\frac{\partial T_1}{\partial t} = \alpha_1\left(\frac{\partial^2 T_1}{\partial x^2} + \frac{\partial^2 T_1}{\partial y_1^2}\right) \tag{1}$$

$$\frac{\partial T_2}{\partial t} = \alpha_2\left(\frac{\partial^2 T_2}{\partial x^2} + \frac{\partial^2 T_2}{\partial y_2^2}\right) \tag{2}$$

and the boundary conditions are

$$\left.\frac{\partial T_1}{\partial x}\right|_{x=0} = \left.\frac{\partial T_2}{\partial x}\right|_{x=0} = \left.\frac{\partial T_1}{\partial x}\right|_{x+\pm L_x} = \left.\frac{\partial T_2}{\partial x}\right|_{x=\pm L_x} = 0 \tag{3}$$

$$T_1|_{y_1=0} = 0 \tag{4}$$

$$k_1\left.\frac{\partial T_1}{\partial y_1}\right|_{y_1=d_1} = k_2\left.\frac{\partial T_2}{\partial y_2}\right|_{y_2=0} \tag{5}$$

$$T_2|_{y_2=0} = T_1|_{y_1=d_1} + R_{\text{th}}k_2\left.\frac{\partial T_2}{\partial y_2}\right|_{y_2=0} \tag{6}$$

$$k_2\left.\frac{\partial T_2}{\partial y_2}\right|_{y_2=d_2} = q''(x,t) = \begin{cases} q''_0\cos(\omega t) & (-w < x < w) \\ 0 & (x < -w, x > w) \end{cases} \tag{7}$$

where $T_i, \alpha_i, k_i, q''_0$ are temperature, thermal diffusivity, thermal conductivity in material i, and the amplitude of the heat flux density at the die-surface, respectively. The resistance, R_{th}, is that at the interface, which is the parameter to be determined by the measurement. The thickness of material i is given by d_i. The periodic heating applied to the die surface is given by (7). For the present study, materials 1 and 2 are aluminum oxide (alumina) and silicon, respectively. Taking $T_i(x, y_i, t) = \tilde{T}_i(x, y_i, \omega)e^{i\omega t}$ and solving $\tilde{T}_i(x, y_i, \omega)$ from (1)–(7), one can determine the amplitude of the surface temperature rise and its phase shift with respect to the heating rate as a function of the heating angular frequency, $\omega = 4\pi f$. The solutions, $\tilde{T}_i(x, y_i, \omega)$ are

$$\tilde{T}_1(x, y_1, \omega) = \sum_{n=0}^{\infty} A_n(n)\cos\left(\frac{n\pi}{L_x}x\right)\sinh(Q_{1n}(\omega)y_1) \tag{8}$$

$$\tilde{T}_2(x, y_2, \omega) = \sum_{n=0}^{\infty}\cos\left(\frac{n\pi}{L_x}x\right)[B_n(\omega)\cosh(Q_{2n}(\omega)y_2) + C_n(\omega)\sinh(Q_{2n}(\omega)y_2)] \tag{9}$$

where

$$A_n(\omega) = q''_0 S[k_2Q_{2n}(\omega)\cosh(Q_{1n}(\omega)\,d_1) \times [\{\tanh(Q_{1n}(\omega)\,d_1) + k_1Q_{1n}(\omega)R_{\text{th}}\} \cdot \sinh(Q_{2n}(\omega)\,d_2) + \cosh(Q_{2n}(\omega)d_2)]]^{-1} \tag{10}$$

$$B_n(\omega) = [\tanh(Q_{1n}(\omega)d_1) + R_{\text{th}}k_1Q_{1n}(\omega)] \cdot \cosh(Q_{1n}d_1)A_n(\omega) \tag{11}$$

$$C_n(\omega) = \frac{k_1Q_{1n}(\omega)}{k_2Q_{2n}(\omega)}\cosh(Q_{1n}(\omega)d_1)A_n(\omega) \tag{12}$$

$$S_n = \begin{cases} \dfrac{w}{L_x} & (n=0) \\ \dfrac{2}{n\pi}\sin\left(\dfrac{n\pi w}{L_x}\right) & (n>0) \end{cases} \tag{13}$$

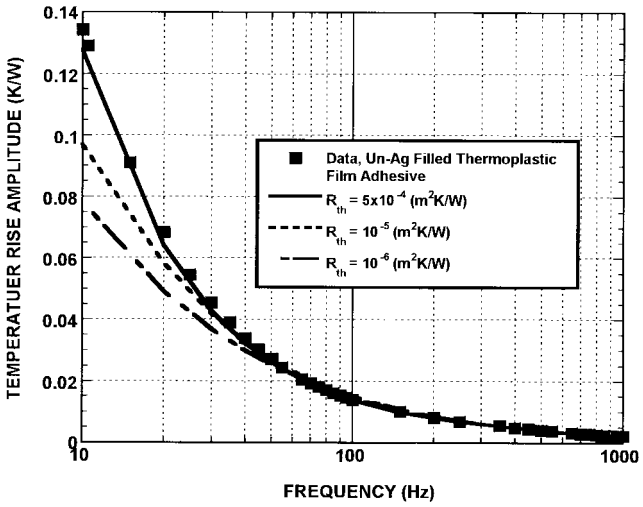

Fig. 4. Amplitude of thermometer temperature rise signal as a function of heating rate frequency.

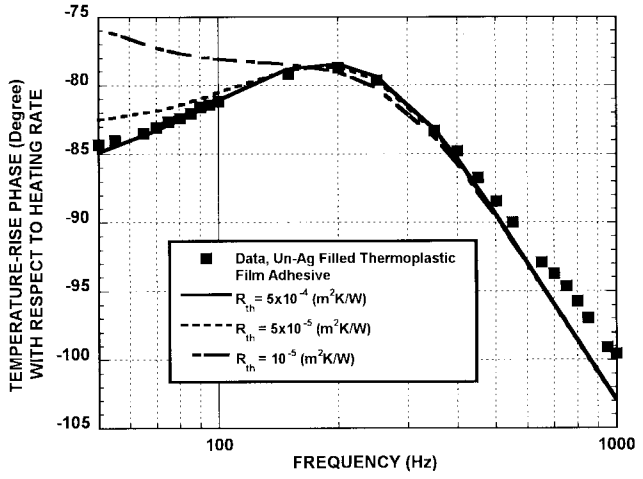

Fig. 5. Phase shift of thermometer temperature rise signal as a function of heating rate frequency.

$$Q_{1n}(\omega) = \sqrt{\left(\frac{n\pi}{L_x}\right)^2 + \frac{i\omega}{\alpha_1}} \tag{14}$$

$$Q_{2n}(\omega) = \sqrt{\left(\frac{n\pi}{L_x}\right)^2 + \frac{i\omega}{\alpha_2}}. \tag{15}$$

The amplitude, $T_A(\omega)$, and the phase shift, ϕ, of the surface temperature rise at the thermometry point are determined using

$$T_A(\omega) = |\tilde{T}_2(x_m, d_2, \omega)| \tag{16}$$

and

$$\tan(\phi) = \frac{\mathrm{Im}(\tilde{T}_2(x_m, d_2, \omega))}{\mathrm{Re}(\tilde{T}_2(x_m, d_2, \omega))} \tag{17}$$

where x_m is the measurement position of the thermometry line when the middle of the heating stripe is taken as $x = 0$.

Figs. 4 and 5 show the predicted amplitude and phase data for the sample structure for varying values of the attachment thermal resistance. At high frequencies above 300 Hz, these curves become identical because the thermal penetration depth in the silicon is smaller than its thickness. At these frequencies, the temperature amplitude and phase are determined only by the thermal properties of the silicon die. In contrast, the predictions differ strongly for frequencies lower than 200 Hz, and it is by means of comparison at these frequencies that the attachment thermal resistance data can be extracted. Figs. 4 and 5 also illustrate this comparison for the case of an epoxy attachment that is not filled with silver particles. The experimental data and the calculated curve are in good agreement except for the phase data at high frequency as seen in Fig. 5. This is caused by the fact that the thermal diffusion length is on the order of the spacing between the heating and thermometry bridges and the thermometry line width for frequencies higher than 500 Hz. In this case, the cross section of the thermometry line cannot be modeled as a point because the phase-shift variation across the line becomes significant. The deviation of the calculation at the high frequency is less clear for the case of the amplitude responses in Fig. 4, considering the measurement uncertainty. A theoretical phase-shift prediction accounting for the line width can be calculated by integrating (9) to obtain a spatially-averaged solution over the thermometry line and using this solution in (17). At the frequencies lower than 200 Hz, this prediction yields less than 0.5% relative difference from to the prediction that ignores the line width, which supports the conclusion that the finite bridge width can be neglected below 200 Hz.

The phase-shift data at low frequencies help reduce the experimental uncertainty in the determination of the attachment resistance. The phase-shift response is most sensitive to thermal resistances between 10^{-6} and 10^{-3} $\mathrm{m^2K/W}$, values that span the range of resistances of typical polymer-based adhesives. The experimental uncertainty is governed by the phase resolution of the lock-in amplifier, which is about 0.01 degrees and yields a relative uncertainty for the resistance measurement that is always less than 2%. The geometrical approximations and the thermal properties for the silicon die and the alumina carrier used for the heat conduction model incur no more than 2% relative error. This yields a total relative uncertainty, determined using the sum-of-squares technique [6], of less than 3%.

It is useful to contrast this value of the uncertainty with the value obtained using a conventional steady-state technique. For the case of a simple one-dimensional steady-state measurement, the thermal resistance of the attachment is

$$R_{\mathrm{th}} = \frac{T_{\mathrm{die}} - T_{\mathrm{carrier}}}{q_0''} - \frac{d_1}{k_1} - \frac{d_2}{k_2} \tag{18}$$

where T_{die} and T_{carrier} are the temperatures at the top surface of the die and at the bottom surface of the carrier, respectively. The heat flux is given by q_0'', d_1, and k_1 are the thickness and thermal conductivity of the die, and d_2 and k_2 are the thickness and thermal conductivity of the carrier. Because most thermometers, including thermocouples and electrical-resistance thermometers, are most precise for measurements of temperature changes, the major problem with this approach is that it is often difficult to ensure that the difference between the temperature rises of the die and carrier is large compared to the temperature rise in the carrier. If this is not the case, the

TABLE I
SPATIALLY-AVERAGED THERMAL RESISTANCE VALUES MEASURED USING FREQUENCY-DOMAIN ELECTRICAL HEATING AND THERMOMETRY

DIE ATTACH ADHESIVE	PROCESS	DIE-ATTACH THERMAL RESISTANCE $\mathbf{R} \times 10^4$ ($\mathbf{m^2KW^1}$)	VOID FRACTION
Ag-Filled Thermosetting Epoxy #1 (complete attach)	Standard Process, cured @180 °C	3.1 ± 0.09	<1%
Ag-Filled Thermosetting Epoxy #2 (incomplete attach)	Standard Process, cured @180 °C	8.9 ± 0.98	35%
Unfilled Thermoplastic Film	Standard Pressure (8 psi)@180 °C	6.8 ± 0.62	<1%
Ag-Filled Thermoplastic Film # 1	Standard Pressure (8 psi)@180 °C	2.5 ± 0.08	<1%
Ag-Filled Thermoplastic Film # 2	Standard Pressure (8 psi)@180 °C, reworked	6.4 ± 0.51	20%
Ag-Filled Thermoplastic Film # 3	Low Pressure (< 2 psi) @180 °C	5.2 ± 0.36	<1%

experimenter is faced with the difficulty of having to take the difference of two relatively large numbers in the numerator of the first term on the right of (18), a problem that dramatically augments the experimental uncertainty. Another problem with the steady-state measurement is that the time required to reach steady conditions can be quite large, due to the large volume of material that must be heated and the relatively large resistance for heat removal to the environment.

Table I provides the die-attach thermal resistances extracted for several different samples using the technique developed here, as well as the void fraction values for the attachment estimated from X-ray images. The values of the resistance vary strongly depending on the attachment process and the adhesive material. The results of lines 1 and 2 in the table show that the technique measures the increase of the thermal resistance due to the existence of voids at the die-attach interface when the samples are prepared using the same adhesive material. The thermoplastic polymer adhesive promises to yield a more uniform attachment than that provided by thermosetting materials for a given set of processing conditions [7], [8]. The data in lines 1 and 4 of the table show that the thermoplastic adhesive yields a lower die-attach resistance than the thermosetting adhesive when no voids are present. This difference may result either from a difference in the intrinsic thermal conductivities of the materials or from the possibility that the thermosetting material formed a thicker layer. The results for the samples of lines 3 and 4 show that the silver-filled adhesive yields a smaller thermal resistance than the unfilled material when the die attachments are fabricated using the same conditions. Table I also provides in line 5 data for a sample with incomplete contact, resulting from several voids that occurred during reworking. The data in line 6 indicate the impact of pressure on the thermal resistance, which is a relevant parameter because it influences both the quality of the contact between the adhesive and the carrier and the die, as well as the thickness of the adhesive.

A lower bound for the die-attach thermal resistance $R_{\rm th}$ can be estimated by assuming that the volume resistance of the adhesive dominates and that the adhesive thermal conductivity is well approximated by the bulk value. Based on this assumption, the die-attach resistance is given by $R_{\rm th} = d_{ad}/k_{ad}$, where d_{ad} and k_{ad} are, respectively, the thickness and the thermal conductivity of the adhesive layer. For the thermoplastic adhesives used for the samples of lines 3 and 4 of Table I, data provided by the vendor [9] indicate that the materials and process used for the samples in lines 3 and 4 of Table I, respectively, form thicknesses of approximately 75 and 125 μm and that the thermal conductivities of the materials are on the order of 0.3 and 3.0 W K^{-1} m^{-1}, respectively. Thus, the lower bound of the resistance is 2.5×10^{-4} m^2 K W^{-1} for line 3 and 4.2×10^{-5} m^2 K W^{-1} for line 4. The measured values are substantially larger, in particular for the case of the silver-filled epoxy. This difference results from uncertainty in the thickness and thermal conductivity of the adhesive, as well as the impedance at the interfaces. While more research is needed to determine which of these problems is most important, the data clearly show that the use of resistance values based on information provided by the vendor companies yield to large errors in the die boundary condition.

III. PHOTOTHERMAL INTERFACE MICROSCOPY (PIM)

While the electrical heating and thermometry discussed in Section II offers exceptional precision in die-attach resistance measurements, it does not provide information about the spatial variation of the resistance in the plane of the die. The local resistance may vary by orders of magnitude within a single die attachment due to voids and partial delamination. These variations yield local hotspots on the die surface, which limit the reliability of the chip. While it is possible to spatially map attachment nonhomogeneity by means of nonthermal methods, such as x-ray and acoustic imaging, these techniques provide no quantitative information about the attachment thermal resistance. The industrial community needs a method that can provide attachment thermal resistance values for direct application in finite-element analysis.

To measure the spatial variation of the thermal resistance, we augment the electrical method described in Section II with photothermal interface microscopy (PIM), which is a calibrated and quantitative extension of more conventional photothermal imaging [10]. Fig. 6 shows a schematic of the experimental facility used for the PIM. While the electrical line experiences heating, as in Section II, the sample is scanned beneath the focus of a diode laser at 640 nm with a spot

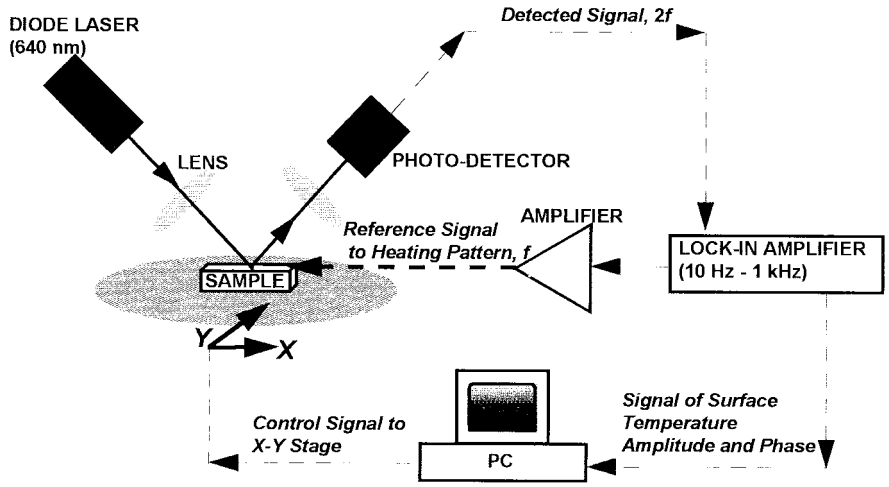

Fig. 6. Apparatus for photothermal interface microscopy (PIM).

size near 50 micrometers. The sample surface heating is modulated at $f = 10$ Hz in the photothermal scanning. Based on the calculation in Section II, this modulation frequency is chosen such that the surface temperature responses are most sensitive to the local die-attach thermal resistance. Since the surface reflectivity of the sample depends on temperature, the amplitude and phase of local temperature fluctuations can be extracted from the photodetector signal using the lock-in amplifier. The signals for the local temperature fluctuations are calibrated by requiring that the spatial average of these signals is identical with the temperature amplitude measured by means of electrical resistance thermometry in the thermometry bridge described in Section II. The relative uncertainty of the temperature amplitude measurement results primarily from uncertainty in the calibration of the thermometry line and is approximately 8 percent.

As the first step of the local thermal resistance extraction process, the die-surface is divided into square area elements, as shown in Fig. 7, whose side length is the same as that of the scanning step, 0.5 mm. The interpretation of the PIM data is complicated by the nonuniformity of the heat generation rate on the top surface of the chip. For this reason, the local heating rate at the die-surface is evaluated using data taken at the relatively high frequency of $f = 1.6$ kHz. The thermal penetration depth at that frequency within the silicon is smaller than the scanning step size, 0.5 mm, which indicates that the data provide a measure of the intensity of local heating. The thermal penetration depth at 1.6 kHz, $L_D = 0.25$ mm, is also less than the silicon die thickness, which indicates that the thermal resistance is not significantly influencing the signal. The purpose of these high-frequency measurements is therefore to map out the spatial variations of heating intensity at the die surface.

The temperature rise at the point $(m, n), \Delta T_{mn}$ is affected by the heating rates of the surrounding points as well as that of its own point and is given by

$$\Delta T_{mn} = \sum_{i,j} F_a(|\vec{r}_{mn} - \vec{r}_{ij}|, R_{\rm th}(m,n)) q''_{ij} \qquad (19)$$

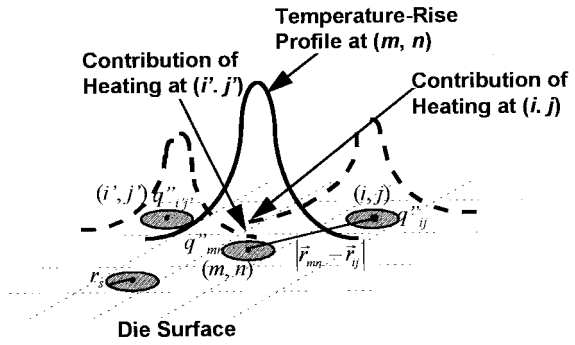

Fig. 7. Geometry used for extracting the local die-attach thermal resistance. The data extraction uses the principle of superposition and assumes that the die-surface heating is composed of multiple heat sources.

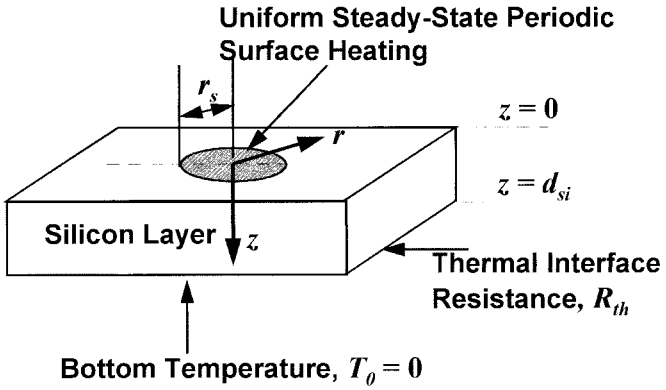

Fig. 8. Schematic representation of the local surface heating model. The lateral dimension is infinite.

where F_a is a solution to the heat equation that describes the impact of the heating rate at the point $(i, j), q''_{ij}$, on the temperature rise at the point (m, n). The parameter $R_{\rm th}(m, n)$ is the local thermal interfacial resistance at the point (m, n). To derive F_a, the heat conduction from the local heating at the die-surface is modeled as shown in Fig. 8. This model

assumes:

1) uniform heat-flux source at each surface measurement point has a circular disk shape whose radius is the same as L_D;
2) temperature is uniform in the carrier;
3) lateral dimension of the chip is infinite;
4) radiative and convective heat losses at the die surface can be neglected.

The governing equation is

$$\frac{\partial T(r,z,t)}{\partial t} = \alpha_{si}\nabla^2 T(r,z,t). \tag{20}$$

The boundary conditions are

$$-k_{si}\left.\frac{\partial T}{\partial t}\right|_{z=0} = q''(r,t) = \begin{cases} q_0'' \cos(\omega t) & (0<r<r_s) \\ 0 & (r>r_s) \end{cases} \tag{21}$$

$$-k_{si}\left.\frac{\partial T}{\partial t}\right|_{z=d_{si}} = \frac{1}{R_{\rm th}}(T|_{z=d_{si}} - T_0) \tag{22}$$

where $k_{si} = k_2, \alpha_{si} = \alpha_2, d_{si} = d_2, r_s = L_D$ is the heat source radius, and $T_0 = 0$ is the temperature of the chip carrier. The temperature-rise amplitude, is obtained in the frequency domain using a Hankel transform [11]

$$\tilde{T}(r,z,\omega) = q_0'' \int_0^\infty d\lambda\lambda J_0(\lambda r)[a(\lambda, R_{\rm th})e^{-\gamma z} + b(\lambda, R_{\rm th})e^{\gamma z}] \tag{23}$$

where

$$a(\lambda, R_{\rm th}) = \left[\frac{J_1(\lambda r_s)}{2k_{si}\gamma}\right]\left(\frac{r_s}{r}\right)(R_{\rm th}k_{si}\gamma + 1)e^{\gamma d_{si}}/[R_{|rmth} \cdot k_{si}\gamma\sinh(\gamma d_{si}) + \cosh(\gamma d_{si})] \tag{24}$$

$$b(\lambda, R_{\rm th}) = \left[\frac{J_1(\lambda r_s)}{2k_{si}\gamma}\right]\left(\frac{r_s}{r}\right)(R_{\rm th}k_{si}\gamma - 1)e^{-\gamma d_{si}}/[R_{\rm th}k_{si} \cdot \gamma\sinh(\gamma d_{si}) + \cosh(\gamma d_{si})] \tag{25}$$

$$\gamma = \sqrt{\lambda^2 + \frac{i\omega}{\alpha_{si}}}. \tag{26}$$

In the above equations, J_0 and J_1, are Bessel functions of the first kind of orders 1 and 2 and λ is the argument for the integral in (23), whose dimension is $m-1$.

The function $F_a(r, R_{\rm th})$ is

$$F_a(r, R_{\rm th}) = \left|\frac{\tilde{T}(r, z=0, \omega)}{q_0''}\right| = \left|\int_0^\infty d\lambda\lambda J_0(\lambda r)[a(\lambda, R_{\rm th}) + b(\lambda, R_{\rm th})]\right|. \tag{27}$$

Secondly, the PIM data at 1.6 kHz are examined to determine the average surface-heat-flux density, $P_{\rm total}/A_d$, where $P_{\rm total}$ and A_d are the total power applied to the heating line on the die surface and the surface area of the die, respectively. The data taken at 1.6 kHz are then examined to determine the local rates of heating, q_{ij}''. These values q_{ij}'' and the local values for the temperature-rise amplitude, ΔT_{mn}, which is taken from the calibrated low-frequency PIM data, are inserted into (19). Finally, (19) is numerically solved with respect to $R_{\rm th}(m,n)$ for each of the 20 × 20 locations on the surface grid. The thermal resistance data are extracted using this procedure are then recorded as a function of position on the die surface.

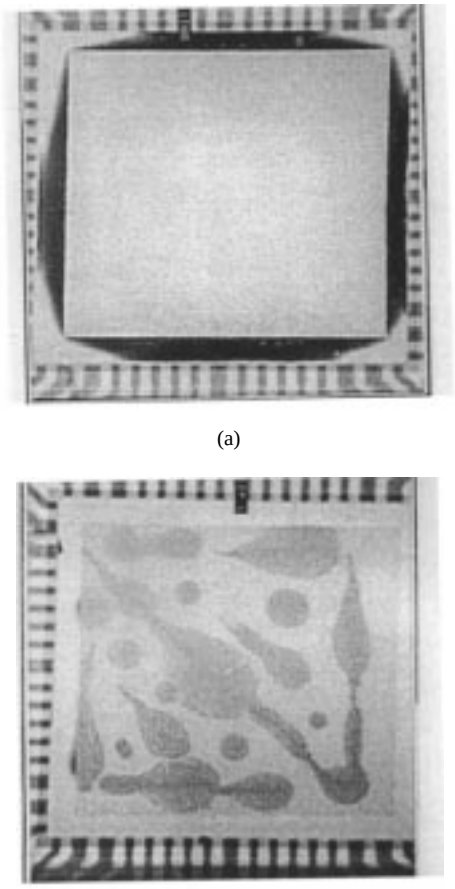

(a)

(b)

Fig. 9. X-ray images of die attachments with varying uniformity: (a) complete attachment and (b) incomplete attachment. The dark portion in (a) shows excess thermosetting adhesive around the die sides. The dark spots in (b) are local contacts of the die made using the adhesive.

Figs. 9 and 10 show x-ray and PIM images of two die attachments of varying quality. Part (a) of each figure shows data for a high-quality complete attachment, while (b) shows data for an attachment that is intentionally made incomplete through the use of insufficient epoxy. Figs. 9(a) and 10(a) do not show any distinct local contrast for the entire attachment area. The darker regions in Fig. 9(b) represent local adhesive contacts in a relatively poor attachment. The PIM images are taken for a die-surface area of about 10 × 10 mm^2, excluding the portions uncovered with the heating metal line. The data on the intermediate surface points are extracted by interpolating those at the surrounding measurement points. This evaluation data process may fail to detect a highly localized variation of the thermal resistance beneath these intermediate points. While the x-ray and PIM images for the case of complete contact are uniform, the images for the incomplete case show

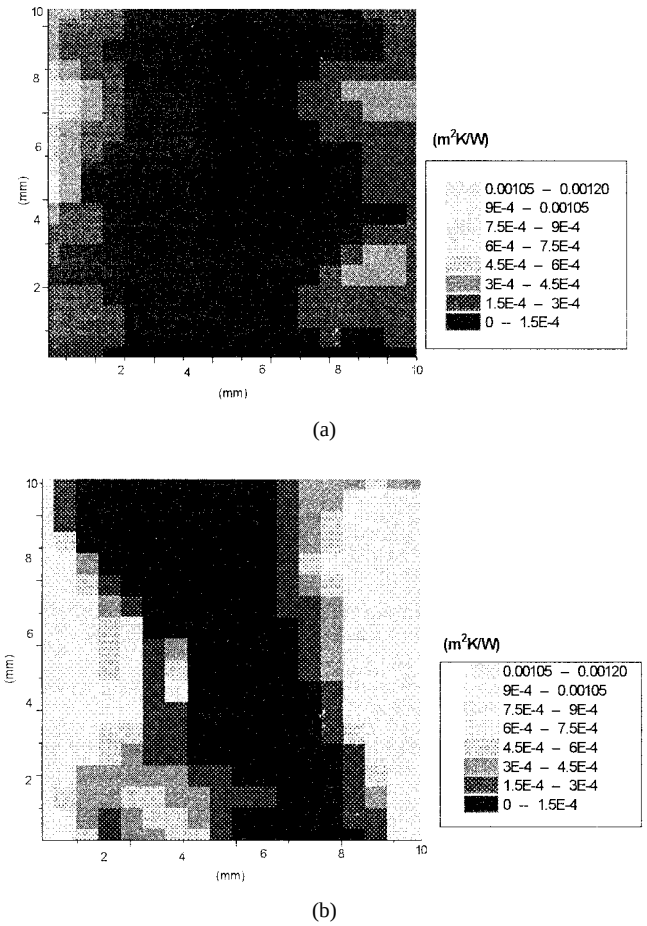

Fig. 10. Photothermal interface microscopy images of die attachments in Fig. 9: (a) complete attachment and (b) incomplete attachment.

a strong spatial variation of the attachment quality. The PIM data indicate that the diagonal attachment line, visible in the x-ray image, reduces the thermal resistance and that the interface areas near the die edges, which have less contacts, yield larger thermal resistance. The lateral thermal healing length in the silicon for the PIM measurement is approximately 2 mm. This means that the current technique has difficulty in detecting a large thermal resistance nonhomogeneity within an area of 2 mm radius since the temperature-rise signal at a data extraction point is affected by the heat spreading from its surrounding points. However, this averaging is important information for design of attachment processes, because it shows that local imperfections of dimension less than about 1 mm will not yield local hotspots at the chip surface. These localized imperfections serve rather to increase the total average temperature rise for a given rate of heating intensity, which is detected using the technique described in Section II. A better mapping resolution can be achieved for a thinner die, in which heat conduction in the normal direction dominates.

IV. Conclusion

The thermal resistance measurement technology described here provides precise, quantitative thermal-property information of direct relevance for finite-element modeling. The uncertainty in the data is exceptionally low because of the comparison of predictions with data over a broad frequency range, and because of the restriction of the heated region to several hundreds of micrometers into the chip carrier. The technology demonstrates the dimensions of attachment imperfections which yield significant temperature variations at the die surface and can be used to provide guidelines for attachment procedures. Because the techniques developed here are nondestructive and noncontact, they are especially well suited for measuring the evolution of the die-attach thermal resistance when the attachment is subjected to repeated heat- or moisture-induced stress. This possibility is a target of ongoing research, which aims to interrogate thermal resistance changes induced by thermal cycling and moisture-induced volume expansion of the attachment. When combined with scanning acoustic microscopy (SAM), the thermal resistance measurement technology described here will facilitate quantitative studies of the relationship of interfacial flaw dimensions and local thermal resistances, particularly if thin die samples can be employed.

Acknowledgment

The authors would like to thank Dr. G. Hotchkiss, Texas Instruments, Dallas, TX, for providing several of the samples and the x-ray images and Dr. K. Gilleo, Alpha Metals, for providing thermoplastic adhesives and helpful technical comments.

References

[1] R. J. Ulrich, "Epoxy die attach: The challenge of big chips," *Semiconduct. Int.*, vol. 17, pp. 101–102, 104, 106, 1994.

[2] K. F. Khory, "The impact of die bond voids in power semiconductor devices on thermal resistance and long term reliability," in *Proc. Int. Symp. Microelectron.*, Atlanta, GA, Oct. 6–8, 1986, pp. 275–80.

[3] G. Pfannschmidt, "Ultarsonic microscope investigations of die attach quality and correlations with thermal resistance," *Qual. Rel. Eng. Int.*, vol. 8, pp. 243–246, 1992.

[4] M. Beyfuss, J. Baumann, and R. Tilgner, "Photothermal imaging of local thermal resistances," *Photoacoustic and Photothermal Phenomena II*, J. C. Murphy, J. W. Maclachlan-Spicer, L. Aamodt, and B. S. H. Royce, Eds. Berlin, Germany: Springer-Verlag, 1990, pp. 17–20.

[5] B. Chambers and T. T. Lee, "A numerical study of local and average natural convection Nusselt numbers for simultaneous convection above and below a uniformly heated horizontal thin plate," *J. Heat Transf.*, vol. 119, pp. 102–108, 1997.

[6] S. J. Kline and F. A. McClintock, "Describing uncertainties in single-sample experiments," *Mech. Eng.*, vol. 75, pp. 3–8, 1953.

[7] K. Gilleo, T. Cinque, S. Corbett, and C. Lee, "Thermoplastic adhesives—The attachment solution for multichip modules," in *Proc. Int. Electron. Packag. Conf.*, San Diego, CA, Sept. 12–15, 1993, pp. 232–242.

[8] S. J. Corbett, K. Gilleo, T. Cinque, M. Corey, and C. Lee, "Thermoplastic die attach adhesives for today's packaging challenges," in *Proc. SAMPE 7th Int. Electron. Mater. Process Conf.*, Parsippany, NJ, June 20–23, 1994, pp. 509–16.

[9] Alpha Metals Inc., *Material Data Sheet of STAYSTIKTM thermoplastic adhesives*.

[10] A. Rosencwaig, J. Opsal, W. L. Smith, and D. L. Willenborg, "Detection of thermal waves through optical reflectance," *Appl. Phys. Lett.*, vol. 46, pp. 1013–1015, 1985.

[11] H. S. Carslaw and J. C. Jaeger, *Conduction of Heat in Solids*. London, U.K.: Oxford Univ. Press, 1959.

Katsuo Kurabayashi received the B.S. degree in precision machinery engineering from the University of Tokyo, Japan, in 1992, and the M.S. and Ph.D. degrees in materials science and engineering from Stanford University, Stanford, CA, in 1994 and 1998, respectively.

His work focuses on the measurement and modeling of thermal transport properties of electronic packaging and organic materials for advanced integrated circuits. He spent the summer of 1997 as an Intern with the Components Research Group, Intel Corporation, Santa Clara, CA.

Kenneth E. Goodson received the B.S., M.S., and Ph.D. degrees from the Mechanical Engineering Department, Massachusetts Institute of Technology, Cambridge, MA, in 1989, 1991, and 1993, respectively.

He is an Assistant Professor and Terman Fellow with the Mechanical Engineering Department, Stanford University, CA. For 16 months, starting in 1993, he was with Daimler–Benz AG, Germany, where he worked on the application of CVD diamond layers for the cooling of high-power automotive electronics. He joined Stanford University in 1994, where he now supervises eight Ph.D. students studying thermal phenomena in electronic micro- and nanostructures.

Dr. Goodson received the ONR Young Investigator Award and the NSF CAREER Award.